Structural Health Monitoring (SHM) using torsional guided wave EMATs

Journal Title
XX(X):1–11

DOI: 10.1177/ToBeAssigned
www.sagepub.com/

Balint Herdovics and Frederic Cegla

Abstract

Torsional guided wave inspection is widely used for pipeline inspection. Most commonly piezoelectric and magnetostrictive transducers are used to generate torsional guided waves. These types of transducers require bonding or mechanical contact to the pipe which can result in changes over time which are undesirable for Structural Health Monitoring. This paper presents a non-contact Lorentz force based Electromagnetic Acoustic Transducer for torsional guided wave monitoring of pipelines. First, the excitation mechanism of the transducer is simulated by analyzing the eddy current and the static magnetic field using the finite element method. An EMAT transformer model is presented which describes the eddy current generation transfer function and the ultrasound excitation. Independently simulated eddy current and magnetic fields are used to calculate the Lorentz force that an EMAT array induces on the surface of a 3 inch schedule 40 pipe and an explicit finite element solver is then used to simulate the elastic wave propagation in the pipe. Then, the reception mechanism and the expected received signal levels are discussed. The construction of an experimental transducer is described and measurement results from the transducer setup are presented. The measured and modeled performance agree well. Finally, a monitoring example is presented where an artificial defect with 3% reflection coefficient is introduced and successfully detected with the designed sensor.

Keywords

Guided wave, Torsional wave, Structural Health Monitoring, Baseline subtraction, Electromagnetic Acoustic Transducer

Introduction

Guided wave ultrasound in pipes

Guided wave testing is widely used for non-destructive Evaluation (NDE) as the travelling wave covers large distances, and fewer measurements are needed to inspect large structures (1). The guided waves are confined within the boundaries of the structure (waveguide) which results in increased ultrasound propagation range compared to bulk waves which suffer from beam spread related energy loss.

An infinite number of guided wave modes can propagate in a structure. The properties of guided wave modes depend on the material properties and the geometry of the structure. The analysis of key properties such as dispersion curves (phase velocity and group velocity) are well known for plates and pipes. (2). The dispersion curves generated using the Disperse® software (3) for a 3 inch Schedule 40 mild steel pipe are shown in Figure 1.

The modes which can propagate in pipe-like structures are the longitudinal L(x,y), the flexural F(x,y) and the torsional modes T(x,y), where x stands for the circumferential order and y denotes the mode number. The majority of these modes are frequency dependent and will result in dispersive wave propagation. The amplitude of the dispersive waves decreases, and the wave packet lengthens during their propagation. The only wave mode which is frequency independent in the whole frequency region is the zero order fundamental torsional mode T(0,1).

In the 1990's the L(0,2) mode was used for guided wave inspection by Alleyne et. al as the phase velocity of this mode is relatively constant in medium and high frequencies

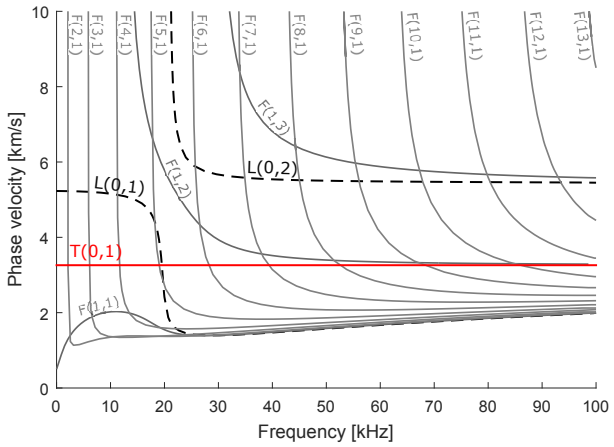

Figure 1. Dispersion curves for a 3 inch mild steel pipe showing the phase velocity of the longitudinal, flexural and torsional modes under 100 kHz.

(4; 5). In later years the zero order tosional mode became more popular. Although some researchers investigated the possibility of higher frequency excitation (around MHz range) (6), the frequency of guided waves employed in practical testing are usually lower than 100 kHz. Higher order torsional modes are not present in this frequency range as the cut-off frequency of the higher order torsional modes is around 300 kHz (7; 8). The displacement of the fundamental torsional mode is almost uniform along the pipe wall therefore it is equally sensitive to defects and cracks at any location along the pipe wall thickness (9).

The interaction of the torsional wave T(0,1) mode with defects and pipe features has been widely studied. Axisymmetric features (i. e. welds and uniform wall thickness changes) only reflect axisymmetric modes. When the operating frequency is below the cut-off frequency of the higher order torsional modes no mode conversion occurs from axisymmetric features. The interaction is usually described by the reflection coefficient which is calculated as the ratio of the reflected wave amplitude and the amplitude of the incident wave. However, the defects are usually non-axisymmetric and their ultrasound response is more complex. A portion of the incident wave is still reflected, but also mode conversion occurs and other modes (e.g. flexural modes) can be reflected. The reflection of the torsional mode caused by cracks and notches have been studied by Demma et al.(10). He investigated the parameters (like circumferential, axial extent, frequency) which affect the reflection coeffient. Carandente has concluded several finite element simulations to further increase the knowledge of the torsional wave reflection from complex defects (11). Galvagni investigated the effect of pipe supports at different loading conditions and discussed the reflection and mode conversion of the supports (12).

The researchers have reported that the torsional wave reflection coefficient of defects is dependent on the cross sectional area loss, and the correlation function is roughly linear. Therefore the defect size can be estimated from the reflection coefficient magnitude.

Companies have developed commercially available guided wave transducers. Guided wave Testing is now well established as a test method in industry, with equipment being sold by several companies (13; 14; 15).

Structural Heatlh Monitoring strategies

Traditionally, ultrasound inspection has been carried out in discrete inspections, each time access is gained to the inspected structure and a single shot measurement is carried out. Nowadays, a new trend is to use permanently installed transducers where measurements can be initiated remotely and the recorded data is sent back to the operators.

This is cost effective, as the cost of access often exceeds the cost of an NDE measurement. For example to gain access to some plant locations scaffolding needs to be built, roads or earth needs to be dug up or insulation removed. With permanently installed transducers access is only required once and subsequent measurements do not required additional access costs. Furthermore, the permanently installed transducers allow more frequent measurements to be taken, increasing the chance to detect a newly developing defect. Even further, during the monitoring process, the difference between ultrasonic signals can result in gaining detailed knowledge about changes in the structure that are not available from a single ultrasound measurement itself. The monitoring strategy which is implemented to detect small changes in the structure using permanently installed transducers is commonly termed Structural Health Monitoring (SHM).

The most common signal processing method for monitoring is the baseline subtraction. The baseline ultrasound signal is collected in an early measurement, when the structure's health condition is known. This baseline signal is then compared with the later measurements (often termed readings). Developing defects and corrosion alter the ultrasound wave propagation and the change in the ultrasonic signal can be identified. Unfortunately, Environmental and Operational Conditions (EOC) also affect the ultrasound propagation and the baseline subtraction method without EOC compensation is ineffective in industrial applications (16). The loading of the structure at supports and the temperature variations influence the wave propagation and the recorded ultrasonic signal is altered. It has been reported that usually the change in the structure's temperature have the biggest effect on the ultrasound time signal (17). The temperature changes the propagation speed of the ultrasound and results in different arrival times for each echo. The subtraction of echoes with slightly different arrival times will result in a small residual signal which is difficult to differentiate from the echo of a defect and therefore the defect monitoring ability is reduced.

Various compensation methods and signal processing techniques (18; 19; 20) have been developed to overcome the effect of EOC and make SHM possible.

Transducers

The SHM strategies perform advanced methods for defect monitoring. They all rely on transducers which can generate and receive ultrasonic signals with high repeatability/stability. With a stable transducer the change in the ultrasonic measurement refers to a change in the structure. However, any instability in the transducer or its bonding will also result in a change of the excited and measured signal. The changes in the ultrasonic signals can either be a result of the presence of small defects that should be detected, but they are also easily confused with changes in the transducer's transfer function. Piezoelectric transducers are widely used for ultrasound generation as they excite strong signals. Most commonly adhesive bonding is used to attach the piezoelectric crystal to the test specimen. The stability of these bonded piezoelectric transducers was investigated by researchers (21). Attarian et al. reports that the bonding adhesives can degrade over long time period when they are exposed to cyclic thermal load (22). As high temperature variations are expected in industrial applications (for example pipes carrying varying temperature fluids) the use of adhesively bonded transducers can result in instability and drifts. While Electromagnetic Acoustic Transducers are usually referred to as contactless transducers, this is not true for the magnetostrictive types of EMATs which are usually used with a bonded highly magnetostricitve strip (23; 24)–. The use of a magnetostrictive strip enhances the excited wave strength but sacrifices the contactless feature of the transducer (25).

Lorentz force based EMATs operate contactlessly as the wave excitation is caused by the interaction of the static magnetic field and the eddy current inside the test specimen. Therefore, their stability over long time periods is expected to be better than conventional bonded transducers, but they excite weak signals. This makes implementing a Lorentz force based EMAT with sufficient Signal-to-Noise SNR ratio more challenging. There are further advantages of the use of EMATs such as the ease of deployment and installation. There are also disadvantages such as the

increased complexity of the transduction mechanism and the potential influence of temperature on the excited signals. In the past it is often also quoted that very high powers are required to drive EMATs which might make them unsuitable for use in restricted areas where intrinsic safety is required. Nonetheless, this paper shows that if EMATs are carefully designed then low power operation can yield sufficient SNR to carry out successful testing.

Electromagnetic Acoustic Transducer for zero order torsional wave excitation

This paper investigates the possibility of using an EMAT based measurement system for pipeline Structural Health Monitoring. It is our aim to design an array of EMAT coils that can excite and sense the zero order torsional mode with 40 dB mode purity. The 40 dB (factor of 100) suppression in the amplitude of the unwanted modes in the time signal (often referred to as coherent noise) is sufficient for most practical applications. The proposed EMAT array prototype is shown in Figure 2, where the EMAT elements are evenly distributed along the circumference of the pipe, and each element generates a tangential force on the pipe. The forces are generated on discrete surface locations as the coil shape prevents a uniform tangential excitation load around the circumference.

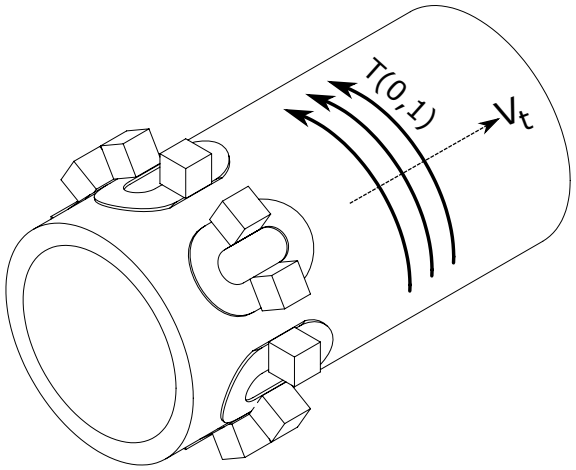

Figure 2. Zero order torsional wave (T(0,1)) excitation: Several EMAT elements placed on the circumference of the 3 inch NPS pipe.

Figure 1 on page 1 shows that several modes exist in a pipe at the frequency region under 100 kHz. The flexural and longitudinal modes can exist alongside the relevant torsional wave. The longitudinal modes are suppressed as no axial force is applied to the pipe surface by the transducer. However, as the tangential forces are applied on discrete surface areas the generation of flexural modes is possible. Appropriate transducer design is required (see Section on page 5) to suppress the flexural modes in the pipe.

The defect monitoring capability can be further enhanced by using two rings of EMAT placed within a specified distance. Employing the two rings a directional control algorithm can be used to send waves selectively in either direction (26; 27). Exciting both rings of the transducer enables the generation of waves that constructively interfere when they propagate in one direction but destructively interfere and cancel out when traveling in the other. With the directional control the exact location of the echo source can be determined; whereas without directional control the received echo could be originating from either the left or the right side of the transducer.

To quantitatively understand the excitation mechanism simulations where employed. In order to reduce computation time and simplify the calculations, the simulations are split into several sub problems. The force generated by an EMAT element is calculated first. The generated ultrasound waves caused by evenly distributed EMAT array elements will be investigated in a separate simulation afterwards.

EMAT force generation model

Electromagnetic transducers can generate acoustic waves by different transduction mechanisms. Magnetostrictive, magnetization and Lorentz force transducers are used for wave excitation (28). Magnetostriction and magnetization only occurs in ferromagnetic media, while the Lorentz force transducers can be used on all conductive materials (28). Usually both the magnetostrictive and Lorentz forces are generated on ferromagnetic media. The dominant force generated by a transducer is dependent on the EMAT configuration and the material properties (25). This paper introduces a Lorentz force based transducer and neglects the magnetostrictive and magnetisation forces. The Lorentz force EMATs generate the ultrasonic wave from the interaction of the static magnetic field and the eddy current in a conductive material. The static magnetic field is usually generated by a permanent magnet, whilst the eddy current is generated by the alternating magnetic field of a current carrying coil. The resulting force density $\underline{\boldsymbol{f}}$ is calculated by the cross product of the eddy current density $\underline{\boldsymbol{J}}$ and the static magnetic field $\underline{\boldsymbol{B}}$:

$$\begin{bmatrix} fx \\ fy \\ fz \end{bmatrix} = \begin{bmatrix} Jx \\ Jy \\ Jz \end{bmatrix} \times \begin{bmatrix} Bx \\ By \\ Bz \end{bmatrix} = \begin{bmatrix} J_y B_z - J_z B_y \\ J_z B_x - J_x B_z \\ J_x B_y - J_y B_x \end{bmatrix} \tag{1}$$

An array of EMATs containing identical elements will operate together to generate the torsional wave. The force generated by an element of the EMAT array is simulated on a conductor plane (Making the simulation on a planar conductor is a reasonable assumption as the pipe radius is large). Consider a planar coil elongated in the x direction and two permanent magnets placed onto the straightened section of the coil as shown in Figure 3.

This assembly is placed onto a conductive, highly permeable material (e.g. mild steel). In order to calculate the force generated by the EMAT first the static magnetic field is simulated; then the eddy current flow is analyzed. The force is then estimated by combining the result of these independent simulations.

Static magnetic field A 3D simulation was carried out in COMSOL Multiphysics® Modeling Software (29) to evaluate the static magnetic field generated by the permanent magnets. 12 mm cubic magnets were modeled 1 mm above the 5 mm thick mild steel plate. The magnets had differently

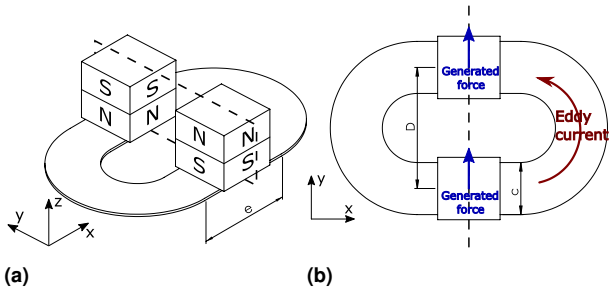

Figure 3. The EMAT transducer assembly consisting of a planar elongated current carrying coil and a permanent magnet shown in three-dimensional view (a) and shown from above the planar coil (b). The eddy current flow and the force generated in a conductive substrate is indicated in (b)

orientated remanent magnetization (1.4 Tesla). The magnetic field with the streamlines on the symmetry plane are shown in Figure 4a. Despite the permanent magnet's vertical magnetization, the magnetic field lines are tilted relative to the vertical remnant magnetization as they form a closed loop. Furthermore, due to Snell's law the magnetic field lines are further diffracted when they enter into a highly permeable material (μ_r~100 in this case). This results in a large horizontal component of the magnetic field in the mild steel. The vertical (z) and horizontal (y) component of the static magnetic field 10 μm under the mild steel surface is shown in 4b. The y component of the static magnetic field in the central region of the magnet can be reduced by using bigger magnets, but cannot be totally eliminated.

Eddy current simulation The eddy current flow induced by a 34 turn coil on a mild steel material was simulated using COMSOL Multiphysics® Finite Element software. The coil lift-off of 100 μm was used in the simulations. The coil input current was set to a 1 A 30 kHz harmonic signal. The simulation revealed that the shape of the eddy current flow is similar to the coil's shape. The current flow has a straight section underneath the coil's straightened section. The coil elongation parameter (denoted by e in Figure 3) therefore was set to 25 mm so that the static magnetic field of the permanent magnet can only interact with a straight flow of eddy current. The effect of changing the coil width (parameter D) and width of the wire tracks (parameter c) was investigated. It was concluded that the eddy current flow is easy to manipulate by changing the coil dimensions. The magnitude of the eddy current density flowing through the symmetry plane (indicated by a dashed line in Figure 3) is plotted in Figure 5 when the coil mean diameter is set to 20, 25, 30 mm (a) and the coil track width is set to 7, 10, 13 mm (b). Note, that the total eddy current did not change whilst varying the coil dimensions. It can also be seen that the highest current density flows under the central turns of the coil.

The frequency of the excitation current has little effect on the shape of the eddy current, however it changes the eddy current skin depth. The eddy current magnitude in the conductor is decreasing exponentially as a function of distance from the surface; at the skin depth it is decreased by 63% (factor of 1/e). The skin depth is dependent on the

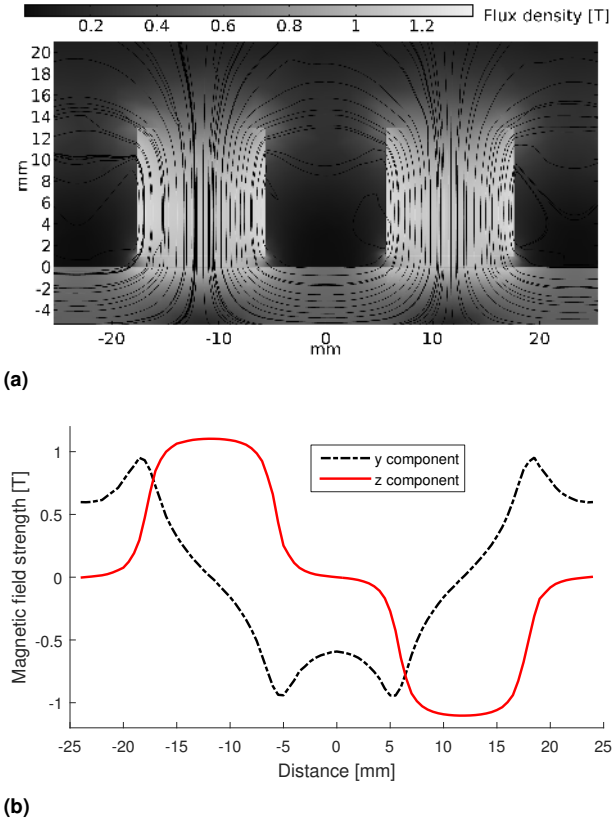

Figure 4. Simulated static magnetic field generated by two Neodymium (NdFeB) magnets whose remnant magnetization strength is 1.4 Tesla and magnetization direction is in the vertical (z) direction with opposite polarity: (a) Magnitude of the static magnetic field strength and field lines generated by the 12mm cubic magnets on a 5 mm mild steel plate. (b) The horizontal (y) component and the vertical (z) component of the static magnetic field in the mild steel plate near the top surface.

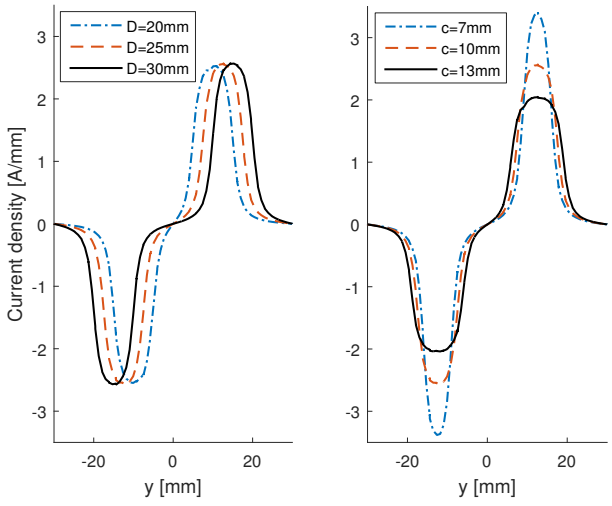

Figure 5. Simulated eddy current density at the symmetry plane of the EMAT when the coil dimensions are varied. The coil width (parameter D) is set to 20, 25, 30 mm (left); the width of the coil turns (parameter c) is set to 7, 10, 13 mm. The simulation frequency of 30 kHz was used.

excitation frequency f, the resistivity ρ and the permeability μ of the conductor in which the eddy current is induced (30).

$$\delta = \sqrt{\frac{\rho}{\pi \cdot f \cdot \mu}} \tag{2}$$

The skin depth in a mild steel conductor for a 30 kHz signal is around 120 µm.

Generated force The physical constraints of the eddy current flow imposed by the elongated coil design (straight flow in x direction at the area where the magnets are placed) will lead to a simplified expression for the body force:

$$\begin{bmatrix} fx \\ fy \\ fz \end{bmatrix} = \begin{bmatrix} Ix \\ 0 \\ 0 \end{bmatrix} \times \begin{bmatrix} Bx \\ By \\ Bz \end{bmatrix} = \begin{bmatrix} 0 \\ -J_x B_z \\ J_x B_y \end{bmatrix} \tag{3}$$

The skin depth of the eddy current in mild steel is relatively small (~120 µm at 30 kHz). As the three-dimensional body force acts on a thin volume near the surface of the conductor it is approximated by a two-dimensional surface traction vector. The assumption is appropriate because the magnetic field change is small in this region.

The generated y and z component surface forces are numerically calculated and are shown in Figure 6 on the symmetry plane of the coil that is normal to the x-direction. The existence of the vertical component of the force is well known for EMATs, see for example (28). The force amplitude is very small, meaning that only low amplitude displacements are expected. The y (horizontal) component of the surface force at different distances (0 to 6 mm) from the symmetry plane is shown in Figure 7. The plot indicates that the relevant area where the EMAT generates a force is around 10 mm by 10 mm (as the surface force decreases rapidly at the distance of 5 mm from the symmetry plane).

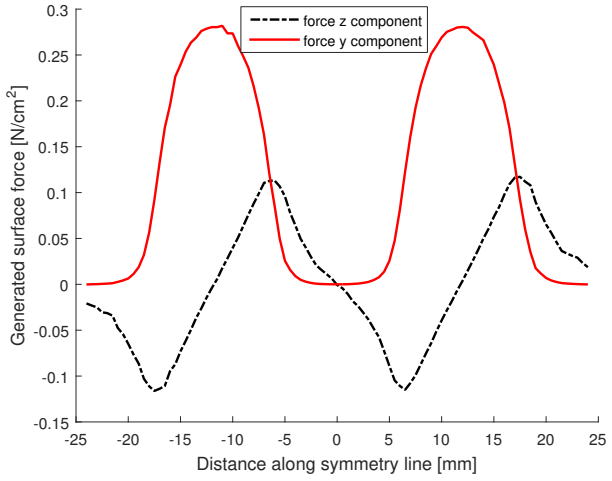

Figure 6. The simulated horizontal y component and the vertical z component of the EMAT generated surface force at the symmetry plane location. The symmetry plane is shown in Figure 3 with dashed line.

Torsional wave generated by an array of EMATs

An array of EMAT coils can be used to excite the fundamental (zero order) torsional wave (T(0,1)) on cylindrical structures such as pipes. In this document we consider the excitation of a 3 inch Schedule 40 NPS pipe. The actual outer diameter of the pipe is 3.5 inch (88.90 mm) and the wall thickness is 0.216 inch (5.486 mm). Several transducer elements are placed around the circumference of the pipe, as shown in Figure 2 on page 3.

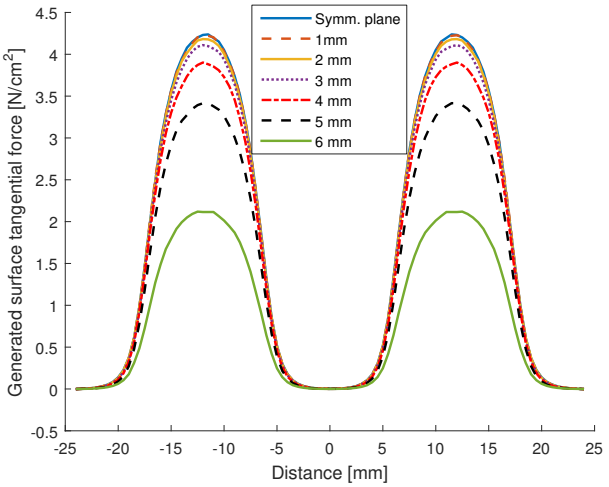

Figure 7. Simulated force in horizontal direction (y component) of the EMAT at the symmetry plane, and on parallel planes at evenly spaced distances from the symmetry plane.

The 6 coil, 12 magnet EMAT coil array placed around the pipe will generate a force which is a periodic function along the circumference. The tangential (Equation 4) and radial forces (Equation 5) in function of the angle (θ) is estimated as the first five component of the Fourier series of the simulated force originally shown in Figure6:

$$f_T(\theta) = \sum_{n=0}^{n=4} a_n \cdot cos(12 \cdot n \cdot \theta) \tag{4}$$

$$f_R(\theta) = \sum_{n=1}^{n=4} b_n \cdot sin(12 \cdot n \cdot \theta) \tag{5}$$

where $a_0 = 0.135\frac{N}{cm^2}$, $a_1 = -0.1811\frac{N}{cm^2}$,$a_2 = 0.0334\frac{N}{cm^2}$,$a_3 = 0.0245\frac{N}{cm^2}$,$a_4 = -0.0095\frac{N}{cm^2}$,$b_1 = -0.1091\frac{N}{cm^2}$,$b_2 = 0.0146\frac{N}{cm^2}$,$b_3 = 0.0147\frac{N}{cm^2}$,$b_4 = 0.0052\frac{N}{cm^2}$,

The first five components of the fourier series estimates the simulated results with an error of 3.6% and 4.3 % for the radial and tangential components respectively. The distribution of the forces along the skin depth was neglected as the skin depth is much smaller than the thickness of the pipe. Therefore, the forces acting on the pipe were set to be surface tractions.

The perfect excitation of the torsional wave would be an uniform tangential force over the whole cross section of the pipe. This is only approximately achievable with EMATs for numerous reasons:

1. The EMAT generates the excitation force only on the surface of the pipe. The surface excitation is adequate as only the fundamental mode is excited when the excitation frequency is below the cut-off frequency of the higher order torsional modes (31). The cut-off frequency of the second order torsional mode T(0,2) is around 300 kHz for this particular thickness (7; 8).

2. As shown above, the EMATs generate the tangential force (previously y component in Figure 6) at discrete patches. Flexural modes might be generated when too few excitation patches are used.

3. Radial forces (z component in Figure 6) act on the pipe surface, which might excite some further flexural modes. It is expected that an increased number of coils reduces the flexural modes that are excited by the radial forces.

Despite the imperfect excitation the transduction arrangement can result in pure wave generation (the suppression of unwanted modes to below -40 dB of the T(0,1) signal amplitude is considered as pure wave generation). The excitation frequency range of 15-60 kHz is considered for excitation (tone-burst signal center frequency), therefore the higher order torsional modes like T(0,2) are not present in this frequency region.

It has been reported that in order to reduce the flexural modes (generated by the discrete tangential forces) more surface tractions should be used than the highest order flexural mode within the operational bandwidth (4; 26) . The cut-off frequency of the F(12,1) mode is around 85 kHz, therefore 12 surface tractions (6 coils and 12 magnets) are suitable for pure torsional wave excitation (less transducer areas might be operational for lower frequency excitation). Other researchers reported that in order to excite a pure mode the distance between the surface tractions should be smaller than half the wavelength (27). On a 3 inch pipe the 12 surface tractions satisfy this criterion as well.

The coherent noise which is present in the time signal due to excitation of other modes was simulated in ABAQUS CAE finite element simulation program. The torsional and radial force distribution along the circumference used as the FE model input is shown in Equation 4 and 5. This force distribution is estimated from the simulated forces originally shown in Figure 6.– The displacement caused by the tangential and radial forces– was monitored 25 cm away from the excitation location. It can be assumed that the torsional wave purity will further increase for longer propagation distances as the amplitude of the unwanted dispersive modes are decreasing during the propagation.

Previous studies revealed that for efficient finite element modelling the mesh size in the simulation should be 10-20 times smaller than the wavelength of the propagating wave (32). This criterion was fulfilled throughout the simulations. The displacement time signal was recorded for the input frequencies of 30, 45, 60 and 75 kHz. The simulated time signals are shown in Figure 8 when the input frequency was set to 45, 60 and 75 kHz. The result for the 30 kHz simulation is not shown in the figure as the coherent noise level further decreases at lower frequency excitation.

The simulations revealed that the requested mode purity of -40 dB was achieved when the center frequency of the excitation signals was below 60 kHz.

Reception of the fundamental torsional wave

Generally publications focus on the wave excitation mechanism of the electromagnetic transducers. Several publications investigate only the excitation mechanism of the EMATs but not the the reception (33; 34; 35; 36).

Some researchers investigated the reception mechanism along with the excitation mechanism (37; 38; 39) .

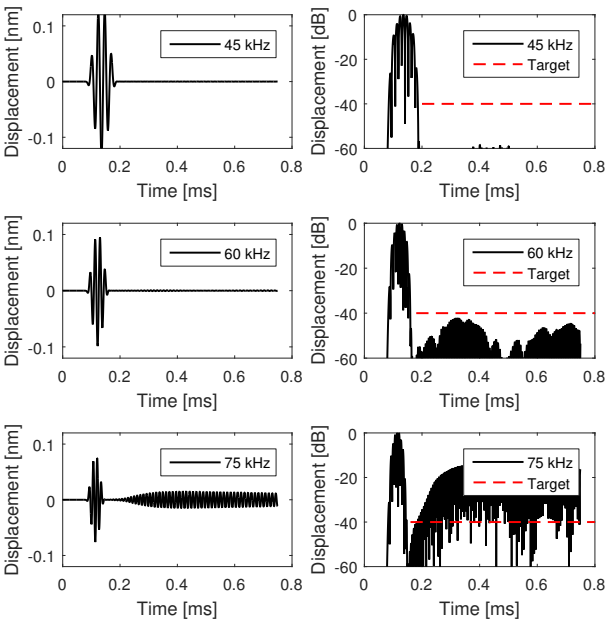

Figure 8. Simulated time signals for 45 kHz (top), 60 kHz (middle) and 75 kHz (bottom) excitation monitored on the 3 inch NPS pipe outer surface 25 cm away from the transducer location. The generated force of an 6 coil EMAT array was used for excitation The left graphs show the displacement in linear scale, whilst the right graphs represent the displacement in decibel scale (normalized to their maximum displacement)

The T(0,1) mode reception mechanism of the EMAT is investigated in this section. Finite Element simulations were carried out simulating linear harmonic displacements of the mild steel conductor underneath the EMAT coils. Since the pipe radius is very large compared to the tangential displacements the linear movement of the conductor and the planar coil (instead of rotation of the curved conductor) is again a reasonable assumption to simplify the analysis.

The modelled reception mechanism is as follows:

The static magnetic field of the magnets (B_0) interacts with the moving particles of the structure and creates an electric field inside it. The generated electric field is described by the inverse Lorentz force and is proportional to the displacement velocity and the static magnetic field. The electromagnetic field generates closed loop currents (J) inside the test specimen:

$$J = \rho \left[E + \frac{\partial u}{\partial t} \times B_0 \right] \tag{6}$$

The magnetic field of the generated current flow will generate voltage inside the coil. In other words, the current caused by the interaction of the static magnetic field and the specimen movement is transformed back into the EMAT coils.

The COMSOL Multiphysics Modeling Software was used to simulate the eddy current inside the specimen. EMAT elements identical to the elements used for excitation were modelled in the FE program. Figure 9 shows the generated eddy current direction and magnitude at the surface of the mild steel conductor when the linear particle movement was set to 1 m/s.

The eddy current flow forms a closed loop circuit. The highest magnitude current flows underneath the magnets.

The receiver coil is well positioned as it overlaps the current flow loop.

The coil elongation parameter can be optimised by finding the best coupling factor between the eddy current and the receiver coils. This optimisation requires running complex simulations and was not studied in details. The elongation of the coil was chosen to be the same as for the transmitter side of the transducer. This results in a relatively good coupling factor between the eddy current flow and the coil, and makes the design and manufacturing process easier.

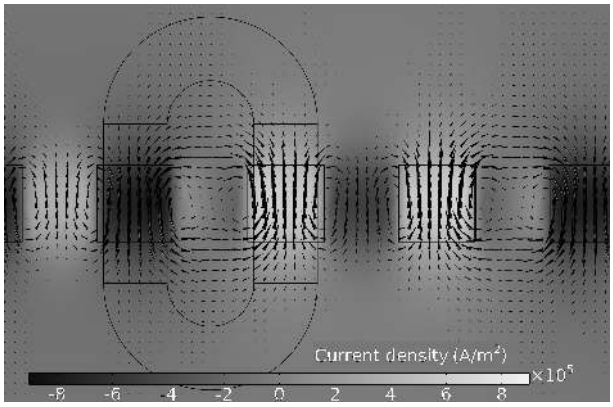

Figure 9. Result of the finite element simulation for the receiver EMAT on a planar surface. The eddy current flow direction is shown by black arrows, whilst the eddy current magnitude is indicated by color plot. The shape of the magnets and one of the coils is shown in faint black lines for reference purposes.

To increase the sensitivity of the EMAT array the coil terminals are connected in series, enhancing the otherwise weak reception of each individual coil.

Emat transformer model and impedance

This section focuses on the induction process and how the signal transfer from coil to eddy current and vice versa is maximized. The eddy current generation principle is shown in Figure 10a. The eddy current generation mechanism is as follows: The changing current in the coil generates changing magnetic flux. A small part of the magnetic flux does not reach the metal conductor, this flux is termed the leakage flux Φ_{S1}). The majority of the flux (Φ_m) penetrates into the metal. The changing magnetic flux generates the eddy current. The eddy current generates a magnetic field. A small part of the eddy current generated flux is a secondary leakage flux (Φ_{S2}) which does not interact with the coil. The rest of the flux opposes the main flux (Φ_m).

As the eddy current generated magnetic flux opposes the flux generated by the coil current , the overall magnetic flux is reduced. The measured inductance of an EMAT coil on a non-ferromagnetic material therefore is lower than the inductance of the same coil in air. The eddy current magnitude in non-ferromagnetic materials can be estimated from the reduction in the measured electric impedance. The eddy current magnitude cannot be estimated this way when it is operated on ferromagnetic materials: both the opposing magnetic field of the eddy current and the ferromagnetic bulk material changes the measured impedance. These two effects cannot be separated.

The EMAT transformer model is presented to analyze the eddy current generation in ferromagnetic materials. This model is then used to estimate the eddy current magnitude using the measured electrical impedance of an EMAT.

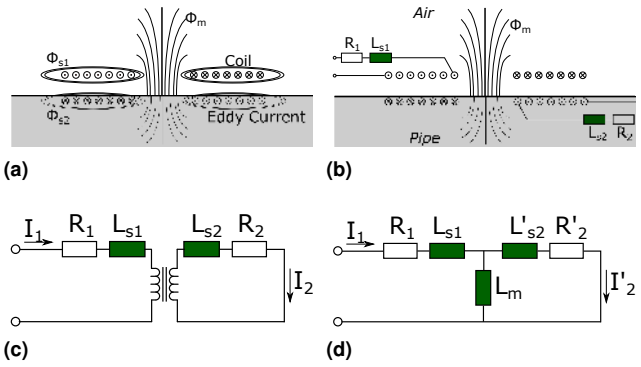

Figure 10. Eddy current generation and steps for deducing the EMAT transformer model circuit diagram. a) physical model of coil, magnetic fluxes and eddy current loop, b) same as a) but showing idealised resistance and inductance of the coil and eddy current loops, c) electrical circuit diagram corresponding to b), d) circuit diagram of c) representing the coupling of coil and eddy current loop via the mutual inductance L_m.

The similarity between an electric transformer and the eddy current generation is evident. The coil behaves as a primary coil, the eddy current flow as a secondary coil. This transformer-like arrangement can be converted into an electrical circuit diagram. First, the resistance of the coil and the eddy current can be expressed as concentrated resistances R_1 and R_2. Furthermore, the leakage fluxes can be concentrated into inductances L_{s1} and L_{s2}. This step is shown in Figure 10b. Now, as the resistances and the leakage inductances are modeled as concentrated parameters the coil and the eddy current flow can be modeled as an ideal transformer. (Figure10c). The eddy current flow is a single turn secondary coil, whereas the coil has N turns. This leads to the third stage of the simplification: the secondary resistance and inductance is reducted, leading to the transformer model circuit representation as shown in Figure 10d. The reducted variables are:

$$R_2' = R_2 \cdot N^2 \tag{7}$$

$$L_{S2}' = L_{S2} \cdot N^2 \tag{8}$$

$$I_2' = I_2 / N \tag{9}$$

The losses in the electric power occur in three different parts of the assembly (40) : (a) power is dissipated in the coil resistance (b) the eddy current flows in resistive material hence power is dissipated in it as well (c) the hysteresis in the magnetization curve results in a loss during the magnetization. The magnetization losses are usually neglected in the calculations as they are small. The power loss in the eddy current was previously calculated by other researchers (41). The EMAT performance increases on low resistivity conductors where less power is lost in the eddy current flow. An important physical constraint in the eddy current magnitude is that the total eddy current must be

smaller than the input current times the number of turns (the opposing magnetic flux of the eddy current must be smaller than the original main flux of the N turn coil):

$$I_2 < I_1 \cdot N \tag{10}$$

Secondly, the power loss inside the EMAT equals the power dissipated in the coil resistance and eddy current flow path.

$$I_1^2 \cdot Re\{Z_{in}\} = I_1^2 \cdot R_1 + I_2^2 \cdot R_2 \tag{11}$$

The resistance of the eddy current flow can be calculated from the resistivity of the mild steel, the dimension of the eddy current flow path and the skin depth. The measured impedance of a single EMAT coil on a 2mm thick mild steel plate from 0-200 kHz is shown in Figure 11.

Using the measured complex impedance information and the calculated R_2 resistance the ratio of the eddy current and the input current can be calculated (see Equation 12). The calculated ratio is compared with Finite element simulations and is shown in Figure 12.

$$\frac{\mid I_2 \mid}{\mid I_1 \cdot N \mid} = \frac{1}{N} \cdot \sqrt{\frac{R_2}{Re\{Z_{in}\} - R_1}} \tag{12}$$

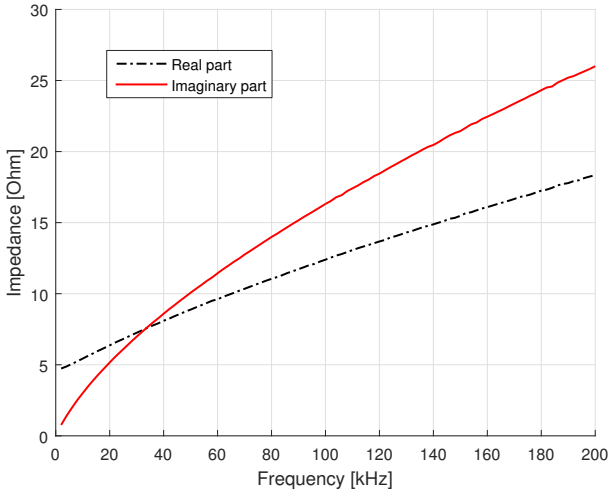

Figure 11. Measured impedance of a 34 turn EMAT on mild steel with minimum lift-off

The hereby presented transformer model can be used for the receiver EMAT array as well. The magnets and the relative motion of the pipe generate an EMF voltage which generate an eddy current. This is then transformed to the coil, and voltage is generated on the coil terminals.

It is expected that a 30 kHz torsional wave with the maximum displacement of $0.205nm$ will generate the voltage of ~2 μV on the receiver EMAT terminals with the output impedance of ~40Ω. (0.205 nm is a typical displacement for a 30 kHz excitation simulated earlier).

Experimental Setup

The excitation signal was generated with a computer based arbitrary function generator and oscilloscope (Handyscope HS3 manufactured by TiePie Engineering ltd, Sneek, Netherlands). This instrument is not capable of generating

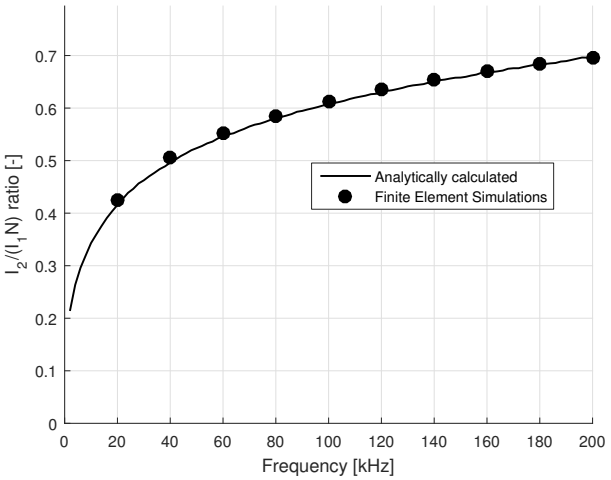

Figure 12. Ratio of the eddy current magnitude and the input current-number of turns product. The analytically calculated values are shown with solid lines, the result of the finite element simulation is shown with dots.

high enough currents to drive the EMAT array therefore a 40 W audio amplifier was used to generate an output signal with low output impedance. The tone-burst center frequency of 27 kHz was selected for measurements. The excitation signal was set to a 5 cycle Hann windowed tone-burst signal. The coil excitation voltage (peak-to-peak) was set to $4V$, which resulted in 900 mA current in the coils.

The low level of output power and the EMAT's poor sensitivity results in extremely weak received signals. A custom made 90 dB analog amplifier was made to amplify the low signal level before connecting it to the receiver channel of the digital oscilloscope. This receiver amplifier was supplied with a 300 kHz low-pass filter to reduce the received electromagnetic noise. The acquired signals are also filtered digitally by a band-pass (16.2 kHz to 33.6 kHz) butterworth filter during the acquisition.

The two transmitter EMAT arrays were placed within 9 cm distance (3/4 wavelength). The receiver array is placed close to the transmitter coils (11 cm) to reduce the dead-zone in the monitoring area.

Acquired signals and Structural Health Monitoring

The manufactured transducer was tested on a 3 meter long 3inch NPS Schedule 40 pipe as shown in Figure 13a. The assembly consisting of two sender and one receiver rings was placed onto the pipe 1m from the right end of the pipe.

The right and left traveling waves are shown in Figure 14. They were computed from signals which were averaged 200 times. Several torsional wave echoes can be seen as they bounce between the pipe ends several times before they are attenuated. The signal purity (coherent noise amplitude relative to the torsional wave amplitude) is above 30 dB.

The excitation RF signal is coupled to the receiver instantaneously at the start of the measurement and is amplified together with the ultrasonic signal. It is often termed cross-talk signal. Because of the low axial separation of the transmitter and the receiver coils the cross-talk signal is larger than the ultrasound signal.

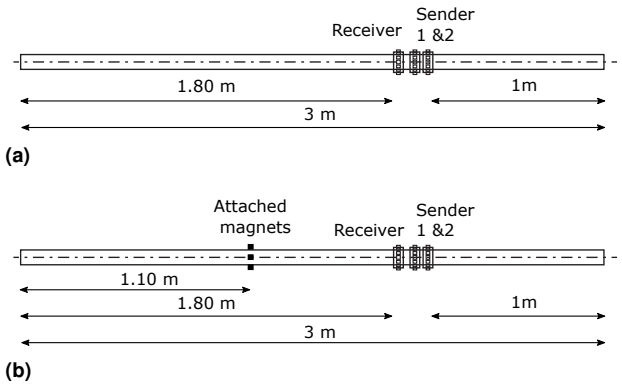

Figure 13. Sketch of the 3 meter long 3 inch NPS schedule 40 pipe used for measurement. The two transmitter and one receiver EMAT arrays are placed 1 meter from the pipe's right end. Signals were acquired on an undamaged (a), and damaged pipe (b). Damage was simulated by the addition of mass (4x 12mm cubed magnets uniformly distributed around the circumference)

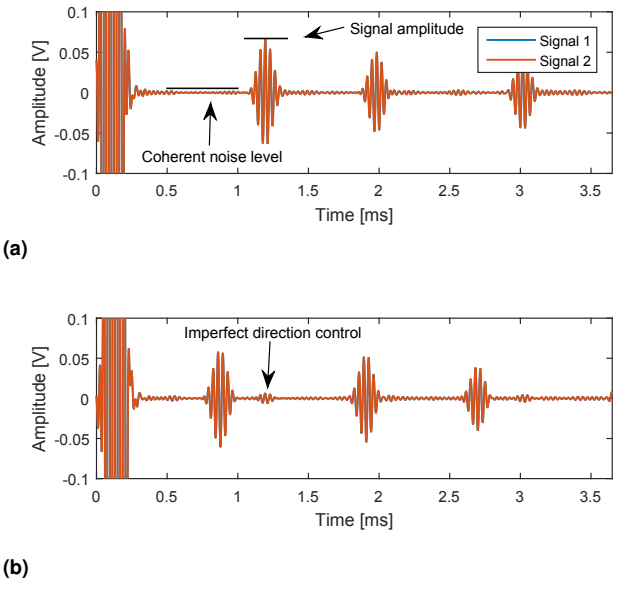

Figure 14. Computed left (a) and right (b) traveling wave propagating on a 3 meter long 3 inch pipe. The echoes seen are the torsional wave reflections from the pipe's end. The stability of the signal is demonstrated as two set of signal (blue and red) are totally overlapping.

When two ultrasonic signals are collected in the same temperature environment and under the same EOC conditions, then the calculated residual signal (difference of the two signals) will only contain random noise. This random noise can be reduced by averaging: the noise reduction is proportional to the square root of the averages. This means that 3 dB reduction in the noise floor can be achieved when the number of averages are doubled. The residual signal level of our acquired signals was 40 dB (factor of 100) lower than the ultrasonic signal amplitude. This indicates that the Signal-to-Noise ratio is 40 dB when the signal is averaged 200 times.

After collecting the baseline signal an extra mass (4 small 12 mm cubic magnets) was joint to the pipe 0.7 m to the left of the transducer to alter the ultrasound propagation (see Figure 13b). The extra mass changes the boundary condition of the surface area where it is placed and it then reflects a tiny portion of the incident torsional wave signal. The extra mass attached to the pipe outer surface have the same effect as a small defect.

The ultrasound signals collected on an undamaged (clean) pipe and on the modified (damaged) pipe are shown in Figure 15a. The torsional wave reflected from the defect is smaller than the coherent noise level. It is only clearly noticeable when the damaged signal is compared to a baseline signal.

The difference of the two signals is better represented in the residual signal, where only the difference of the signals is shown in logarithmic scale normalized to the ultrasonic signal amplitude. A change in the ultrasound can be identified when it rises above the noise floor level. The random noise level in the ultrasonic signal (blue signal in Figure 15b) is less than -40 dB. The residual signal computed from the damaged and clean baseline signal is shown in red in Figure 15b. This residual signal is significantly higher than the noise floor level which indicates a change in the structure.

In monitoring applications the damage call level is chosen to be higher than the noise level, and a potential damage is identified when the residual rises above this threshold. The optimum call level is investigated by researchers in order to maximize the Probability of Detection and minimize the False Alarm Rate. (42; 43).

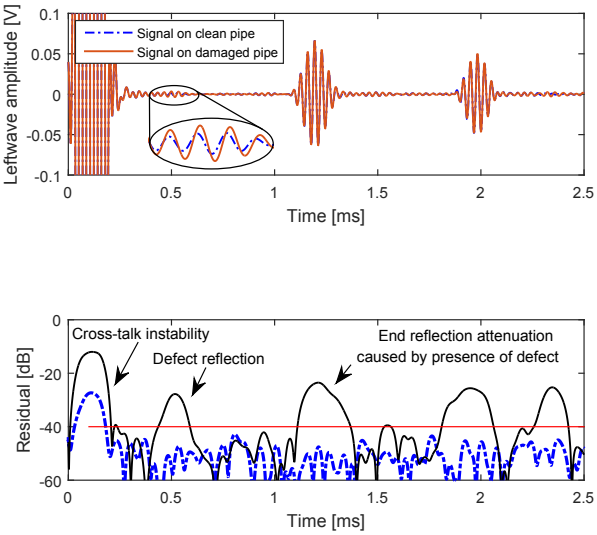

Figure 15. Ultrasonic signals acquired on a pipe before and after introducing an artificial damage (a). Residual signal computed from two clean signals is shown in dashed blue, and the residual signal computed from a clean and damaged signal is shown in black (b).

The ultrasonic signals presented in Figure 15a were collected at constant room temperature, and the EOCs were the same for the measurements. This means that an ideal damage detection scenario was presented which is unrealistic in long-term monitoring. In the long-term the acquired signals will be slightly altered by the changing EOCs. The long-term monitoring capability of the EMAT transducer

is currently being investigated by the authors and will be presented in a future publication.

Conclusions

The aim of this research was to construct a very stable EMAT transducer system for long-term monitoring purposes. Since the transducer operates via a contactless excitation mechanism on a ferromagnetic pipe no adhesive or bonding agents are required. This removes the potential detrimental drift effects that can be often be observed in adhesively bonded transducers. A complete model of the working principle is described from transduction to reception. Finite Element simulations were used to investigate the magnitude of forces and the resulting mode purity that a 6 coil 12 magnet arrangement is capable of generating. The work was focused on the excitation of the fundamental torsional T(0,1) mode in a 3 inch Schedule 40 mild steel pipe. An experimental prototype was built and tested, which performed to expectation. The achieved mode purity was better than 30 dB and an SNR of 40 dB with respect to random noise was achieved by averaging 200 consecutive signal acquisitions.

The system was then used to detect artificially introduced damage (an additional mass) that resulted in a 3% reflection coefficient compared to the full end reflection. The long term stability of the system is currently under investigation. It is believed that the non-contact transduction mechanism of this type of transducer can have significant advantages for the long term structural health monitoring of pipelines.

References

[1] J. L. Rose, Ultrasonic Waves in Solid Media, vol. 107. Cambridge: Cambridge University Press, 2004.

[2] K. F. Graff, Wave motion in elastic solids. Oxford: Oxford University Press, 1991.

[3] B. Pavlakovic, M. Lowe, D. N. Alleyne, and P. Cawley, "Disperse: A General Purpose Program for Creating Dispersion Curve," Annual Review of Progress in Quantitative Nondestructive Evaluation, vol. vol 16, pp. p 185–192, 1997.

[4] D. N. Alleyne, M. J. S. Lowe, and P. Cawley, "The Reflection of Guided Waves From Circumferential Notches in Pipes," Journal of Applied Mechanics, vol. 65, p. 635, sep 1998.

[5] M. J. S. Lowe, D. N. Alleyne, and P. Cawley, "The Mode Conversion of a Guided Wave by a Part-Circumferential Notch in a Pipe," Journal of Applied Mechanics, vol. 65, p. 649, sep 1998.

[6] S. Cho, H. Kim, and Y. Kim, "Megahertz-range guided pure torsional wave transduction and experiments using a magnetostrictive transducer.," IEEE transactions on ultrasonics, ferroelectrics, and frequency control, vol. 57, pp. 1225–9, may 2010.

[7] Z. Liu, J. Fan, Y. Hu, C. He, and B. Wu, "Torsional mode magnetostrictive patch transducer array employing a modified planar solenoid array coil for pipe inspection," NDT & E International, vol. 69, pp. 9–15, jan 2015.

[8] A. Løvstad and P. Cawley, "The reflection of the fundamental torsional mode from pit clusters in pipes," NDT and E International, vol. 46, no. 1, pp. 83–93, 2012.

[9] M. Ratassepp, S. Fletcher, and M. J. S. Lowe, "Scattering of the fundamental torsional mode at an axial crack in a pipe.," The Journal of the Acoustical Society of America, vol. 127, pp. 730–40, feb 2010.

[10] A. Demma, P. Cawley, and M. Lowe, "The reflection of the fundamental torsional mode from cracks and notches in pipes," Acoustical Society of America, 2003.

[11] R. Carandente, Interaction between the Fundamental Torsional Guided Wav PhD thesis, Imperial College London, 2011.

[12] A. Galvagni, Pipeline health monitoring. PhD thesis, Imperial College London, 2013.

[13] Webpage, "Guided Ultrasonics Ltd.," Retrieved from: http://www.guided-ultrasonics.com/, 2016.

[14] Webpage, "Plant Integrity Ltd," Retrieved from: http://www.plantintegrity.com/, 2016.

[15] Webpage, "MKC NDT," Retrieved from: http://www.mkckorea.com/english.htm, 2016.

[16] C. Dan, P. Kudela, and W. Ostachowicz, "Compensation of Temperature Effects on Guided Wave Based Structural Health Monitoring Systems," Proceedings of 7th European Workshop on Structural Health Monitoring, pp. 355–362, 2014.

[17] T. Clarke, F. Simonetti, and P. Cawley, "Guided wave health monitoring of complex structures by sparse array systems: Influence of temperature changes on performance," Journal of Sound and Vibration, vol. 329, no. 12, pp. 2306–2322, 2010.

[18] G. Konstantinidis, P. D. Wilcox, and B. W. Drinkwater, "An investigation into the temperature stability of a guided wave structural health monitoring system using permanently attached sensors," IEEE Sensors J., vol. 7, no. 5, pp. 905–912, 2007.

[19] A. Croxford, P. Wilcox, B. Drinkwater, and G. Konstantinidis, "Strategies for guided-wave structural health monitoring," Proceedings of the Royal Society A: Mathematical, Physical and Engineering Sciences, vol. 463, no. 2087, pp. 2961–2981, 2007.

[20] A. J. Croxford, J. Moll, P. D. Wilcox, and J. E. Michaels, "Efficient temperature compensation strategies for guided wave structural health monitoring.," Ultrasonics, vol. 50, no. 4-5, pp. 517–28, 2010.

[21] K. R. Mulligan, N. Quaegebeur, P. Masson, L.-P. Brault, and C. Yang, "Compensation of piezoceramic bonding layer degradation for structural health monitoring," Structural Health Monitoring, vol. 13, no. 1, pp. 68–81, 2013.

[22] V. A. Attarian, F. B. Cegla, and P. Cawley, "Long-term stability of guided wave structural health monitoring using distributed adhesively bonded piezoelectric transducers," Structural Health Monitoring, vol. 13, pp. 265–280, feb 2014.

[23] Y. Y. Kim, C. I. Park, S. H. Cho, and S. W. Han, "Torsional wave experiments with a new magnetostrictive transducer configuration.," The Journal of the Acoustical Society of America, vol. 117, no. 6, pp. 3459–3468, 2005.

[24] Y. Y. Kim and Y. E. Kwon, "Review of magnetostrictive patch transducers and applications in ultrasonic nondestructive testing of waveguides.," Ultrasonics, vol. 62, pp. 3–19, sep 2015.

[25] R. Ribichini, F. Cegla, P. B. Nagy, and P. Cawley, "Study and comparison of different EMAT configurations for SH wave inspection.," IEEE transactions on ultrasonics, ferroelectrics, and frequency control, vol. 58, no. 12, pp. 2571–81, 2011.

[26] D. Alleyne, B. Pavlakovic, M. Lowe, and P. Cawley, "The Use of Guided Waves for Rapid Screening of Chemical Plant Pipework," Journal of the Korean Society for Nondestructive Testing, vol. 22, no. 6, pp. 589–598, 2002.

[27] J. O. Davies, Inspection of pipes using low frequency focused guided waves. PhD thesis, Imperial College London, 2008.

[28] M. Hirao and H. Ogi, EMATs for Science and Industry: Noncontacting Ultrasonic Measurements. 2003.

[29] Comsol ® INC, "COMSOL ® Multiphysics ®," 2016.

[30] R. THOMPSON, "Physical Principles of Measurements with EMAT Transducers," in Physical Acoustics, vol. 19, pp. 157–200, 1990.

[31] A. Demma, The interaction of guided waves with discontinuities in structures. PhD thesis, Imperial College of Science, Technology and Medicine, 2003.

[32] M. B. Drozdz, Efficient finite element modelling of ultrasound waves in elastic media. PhD thesis, Imperial College of Science, Technology and Medicine, 2008.

[33] X. Jian, S. Dixon, R. S. Edwards, and J. Morrison, "Coupling mechanism of an EMAT," Ultrasonics, vol. 44, no. SUPPL., pp. 653–656, 2006.

[34] W. Luo and J. L. Rose, "Guided wave thickness measurement with EMATs," Insight: Non-Destructive Testing and Condition Monitoring, vol. 45, no. 11, pp. 735–739, 2003.

[35] M. Seher, P. Huthwaite, M. Lowe, P. Nagy, and P. Cawley, "Numerical design optimization of an EMAT for A0 Lamb wave generation in steel plates," AIP Conference Proceedings, vol. 1581 33, pp. 340–347, 2014.

[36] Y. Wang, X. Wu, P. Sun, J. Li, and J. L. Yugang Wang, Xinjun Wu, Pengfei Sun, "Enhancement of the excitation efficiency of a torsional wave PPM EMAT array for pipe inspection by optimizing the element number of the array based on 3-D FEM," Sensors (Switzerland), vol. 15, pp. 3471–3490, jan 2015.

[37] R. Ribichini, F. Cegla, P. B. Nagy, and P. Cawley, "Quantitative modeling of the transduction of electromagnetic acoustic transducers operating on ferromagnetic media.," IEEE transactions on ultrasonics, ferroelectrics, and frequency control, vol. 57, no. 12, pp. 2808–17, 2010.

[38] P. Wilcox, M. Lowe, and P. Cawley, "Omnidirectional guided wave inspection of large metallic plate structures using an EMAT array," IEEE Transactions on Ultrasonics, Ferroelectrics, and Frequency Control, vol. 52, no. 4, pp. 653–665, 2005.

[39] M. Hirao and H. Ogi, "An SH-wave EMAT technique for gas pipeline inspection," NDT & E International, vol. 32, pp. 127–132, apr 1999.

[40] J.H. Fewkes and John Yarwood, Electricity and Magnetism, by J.H. Fewkes and John Yarwood. London: University Tutorial Press, 1965.

[41] J. Isla, M. Seher, R. Challis, and F. Cegla, "Optimal impedance on transmission of Lorentz force EMATs," in AIP Conference Proceedings, vol. 1706, p. 090012, AIP Publishing, 2016.

[42] J. Michaels, Z. Zalevsky, E. Saat, S. Orbach, V. Mico, and J. Garcia, "Feature extraction and sensor fusion for ultrasonic structural health monitoring under changing environmental conditions," IEEE Sensors Journal, vol. 47, pp. 1–6, nov 2008.

[43] E. B. Flynn, M. D. Todd, P. D. Wilcox, B. W. Drinkwater, and A. J. Croxford, "Maximum-likelihood estimation of damage location in guided-wave structural health monitoring," Proceedings of the Royal Society A: Mathematical, Physical and Engineering Sciences, vol. 467, no. 2133, pp. 2575–2596, 2011.